Structural studies of the tethered N-terminus of the Alzheimer's disease Aβ peptide.

ARTICLE *in* PROTEINS STRUCTURE FUNCTION AND BIOINFORMATICS · OCTOBER 2013

Impact Factor: 2.63 · DOI: 10.1002/prot.24312 · Source: PubMed

PROTEINS
STRUCTURE ■ FUNCTION ■ BIOINFORMATICS

Structural studies of the tethered N-terminus of the Alzheimer's disease amyloid-β peptide

Rebecca M. Nisbet,[1] Stewart D. Nuttall,[1] Remy Robert,[1,2] Joanne M. Caine,[1] Olan Dolezal,[1] Meghan Hattarki,[1] Lesley A. Pearce,[1] Natalia Davydova,[1] Colin L. Masters,[3] Jose N. Varghese,[1] and Victor A. Streltsov[1]*

[1] Materials Science and Engineering & Preventative Health Flagship, CSIRO, Parkville, Victoria 3052, Australia

[2] Department of Immunology, Monash University, Clayton, Victoria 3800, Australia

[3] Mental Health Research Institute, The University of Melbourne, Parkville, Victoria 3010, Australia

ABSTRACT

Alzheimer's disease is the most common form of dementia in humans and is related to the accumulation of the amyloid-β (Aβ) peptide and its interaction with metals (Cu, Fe, and Zn) in the brain. Crystallographic structural information about Aβ peptide deposits and the details of the metal-binding site is limited owing to the heterogeneous nature of aggregation states formed by the peptide. Here, we present a crystal structure of Aβ residues 1–16 fused to the N-terminus of the *Escherichia coli* immunity protein Im7, and stabilized with the fragment antigen binding fragment of the anti-Aβ N-terminal antibody WO2. The structure demonstrates that Aβ residues 10–16, which are not in complex with the antibody, adopt a mixture of local polyproline II-helix and turn type conformations, enhancing cooperativity between the two adjacent histidine residues His13 and His14. Furthermore, this relatively rigid region of Aβ (residues, 10–16) appear as an almost independent unit available for trapping metal ions and provides a rationale for the His13-metal-His14 coordination in the Aβ$_{1-16}$ fragment implicated in Aβ metal binding. This novel structure, therefore, has the potential to provide a foundation for investigating the effect of metal ion binding to Aβ and illustrates a potential target for the development of future Alzheimer's disease therapeutics aimed at stabilizing the N-terminal monomer structure, in particular residues His13 and His14, and preventing Aβ metal-binding-induced neurotoxicity.

Proteins 2013; 81:1748–1758.

Key words: amyloid-β; Alzheimer's disease; Aβ crystal structure; Im7; WO-2 Fab.

INTRODUCTION

Alzheimer's disease (AD) is a progressive neurodegenerative disorder and the most common form of dementia in humans. It is characterized pathologically by the presence of large extracellular amyloid plaques in the brain with the main component of the amyloid plaque being the 39–43-residue amyloid β peptide (Aβ) which is produced by the sequential cleavage of the amyloid precursor protein by β- and γ-secretase. The aggregation of Aβ is deemed the major culprit in AD and although the amyloid plaque is the main pathological hallmark of AD, small-molecular-weight oligomers of Aβ are also thought to exert neurotoxic effects, as they correlate well with cognitive impairment and synaptic dysfunction.[1,2] The Aβ peptide and in particular the disaggregation of Aβ oligomers is therefore a widely accepted therapeutic target in the treatment and prevention of AD.

Structural information on the Aβ peptide required to facilitate the development of therapeutics is, however, limited owing to the propensity of Aβ to aggregate and form a distribution of oligomeric states. Nuclear

Additional Supporting Information may be found in the online version of this article.
Abbreviations: Aβ, beta-amyloid peptide; AD, Alzheimer's disease; CDR, complementarity-determining region; Fab, fragment antigen binding; IgNAR, immunoglobulin new antigen receptors; NMR, nuclear magnetic resonance.

*Correspondence to: Victor A. Streltsov, Materials Science and Engineering & Preventative Health Flagship, CSIRO 343 Royal Parade, Parkville, Victoria, 3052, Australia. E-mail: victor.streltsov@csiro.au
Received 25 January 2013; Revised 28 March 2013; Accepted 3 April 2013
Published online 23 April 2013 in Wiley Online Library (wileyonlinelibrary.com).
DOI: 10.1002/prot.24312

magnetic resonance (NMR) studies account for the majority of the structural information thus far, owing to the difficulty in stabilizing Aβ for crystallization. NMR studies report that residues 1–10 of Aβ are structurally disordered, whereas residues 12–24 and the C-terminal residues adopt a β-turn-β fold.[3–8] Other NMR studies suggest that the secondary structure of the monomeric soluble $A\beta_{12-28}$ is in a temperature-dependent equilibrium between an extended left-handed 3_1 (polyproline II; PPII)-helix and a flexible random coil conformation.[9,10] Also, a mixture of local PPII and *β*-strand conformations has been found in the monomeric form of $A\beta_{1-28}$ in acidic conditions by combined Fourier transform infrared and Raman spectra.[11] According to ^{15}N NMR relaxation studies,[10] the $A\beta_{1-40}$ peptide has two regions with *β*-strand propensity (residues, 16–24 and 31–40), two regions with high PII-helix propensity (residues, 1–4 and 11–15), and two unstructured regions with higher mobility (residues, 5–10 and 25–30) connecting the structural elements. It has been hypothesized that PPII might represent a "killer conformation" in the development of conformational neurodegenerative diseases.[12]

Recently, monoclonal antibodies, binding proteins, and scaffold proteins have been utilized with some success to produce homogenous and soluble Aβ peptide solutions suitable for crystallization. Crystallographic structures have been published which describe Aβ residues Glu3–Asp7,[13] Ala2–Ser8,[14] and Asp1–His6[15] in complex with fragment antigen binding (Fab) fragments of monoclonal antibodies PFA1/PFA2, WO2, and 3D6, respectively. These structures are limited by illustrating only the Aβ residues complexed with the antigen, and by the tendency for the antibody-binding site (paratope) to alter the epitope structure. Alternatively, Aβ residues Lys28–Ala42 fused to Tk-RNase HII revealed the C-terminus of Aβ, adopting a β-conformation.[16] Recently, we described a crystal structure of the Aβ amyloidogenic p3 fragment with residues Val18–Ile41 of the Aβ peptide presented within the CDR3 loop region of a shark IgNAR single-variable domain antibody—a structure which was strikingly different from the previous fibrillar models that describe the Aβ C-terminus as forming parallel, in register *β*-sheets.[17]

Encouraged by the results achieved for the crystallization of the Aβ C-terminus, we sought to use additional protein display scaffolds to aid in the crystallization of the Aβ peptide N-terminus. We selected the Im7 immunity protein: a small (9.8 kDa) and stable protein consisting of four antiparallel α-helical framework and two variable surface-exposed loops.[18] Previously, we have reported the use of Im7 as a loop display scaffold for bacteriophage display[19] where it retains its stability after insertions into loop 1[19] or with N-terminal fusions.[20] Based on these properties, we hypothesized that the Im7 four-helix bundle would present a suitable protein scaffold for presentation and crystallization of the N-terminus of Aβ.

Here, we describe the crystal structure of residues 1–16 of Aβ fused to the N-terminus of Im7 and stabilized with the Fab fragment of the anti-Aβ monoclonal antibody WO2. We show, for the first time, the residues 8–16 of Aβ unbound, a region of great interest owing to its potential metal binding properties. This structure, therefore, has the potential to provide a foundation for investigating the effect of metal ion binding on the structure of Aβ.

MATERIALS AND METHODS

Construction of $A\beta_{1-16}$Im7

The $A\beta_{1-16}$Im7 gene construct was produced by splice-overlap PCR using wild-type Im7 DNA template. DNA amplification used forward oligonucleotide #Aβ_Im7_F3 (5′-CTCGCGGCCCAGCCGGCCATGGCCG ATGCGGAATTTCGCCATGATAGCGGCTAGAAGTGCAT CATCAGAAAAGCGAACTGAAAAATAGTATTAGTGATT AC-3′) in combination with reverse oligonucleotide MW1949 (5′-ATATCTTTAGAGCCTGCGGCCGCGCCC TGTTTAAATCCTGGCTTACCGTTAGCAGCTCGCCAT TC-3′). The resulting DNA cassettes were cloned into *Escherichia coli* periplasmic expression vector pGC[21] in frame with C-terminal dual FLAG affinity epitope sequences, and transformed into *E. coli* TG1 (originally purchased from Stratagene, La Jolla, CA). Individual transformants were verified by DNA sequencing (BigDye® Terminator v3.1, Applied Biosystems, USA) and one validated clone chosen for further study.

$A\beta_{1-16}$Im7 expression and purification

Expression and purification of recombinant $A\beta_{1-16}$Im7 was conducted as described previously.[22] Briefly, TG1 cells were grown in 2xYT medium containing glucose (0.1% w/v) and ampicillin (100 μg/mL) to OD_{600} = 0.4. $A\beta_{1-16}$Im7 expression was induced with 1 m*M* of isopropyl β-D-1-thiogalactopyranoside overnight at 26°C. Cells were pelleted by centrifugation at 4000*g* for 15 min (Beckman JA-10) and the periplasmic fraction was isolated as described previously.[23] Recombinant $A\beta_{1-16}$Im7 was purified by affinity chromatography using an anti-FLAG antibody-Sepharose column (10 × 1 cm) equilibrated in Tris-buffered saline (TBS).[24] Affinity-purified proteins were eluted with 0.1*M* of glycine (pH 3.0) and then separated by gel filtration chromatography on a Superdex 200 10/300 GL column (GE Healthcare) equilibrated in TBS. Purified proteins were verified by MALDI-TOF MS and N-terminal sequencing.

WO2 Fab production

WO2 Fab was produced by papain digestion of the WO2 monoclonal antibody as described previously.[25] Briefly, the WO2 hybridoma[26] was grown and maintained in serum-free medium (Invitrogen). Hybridoma supernatant was passed over a Prosep vA Protein A column (Millipore) and bound immunoglobulin eluted with 0.1*M* of glycine (pH 2.5) and then neutralized with 3*M* of Tris (pH 8.0). Immunoglobulin was further purified by gel filtration chromatography on a Superdex 200 26/20 GF column (GE Healthcare) equilibrated in phosphate-buffered saline (PBS). Fab fragments were produced by papain digestion (Sigma)[27] and separated from Fc fragments by affinity chromatography on a HiTrap rProtein A FF column (GE Healthcare) followed by gel filtration chromatography of the flow-through using a HiLoad 16/600 Superdex 200 column (GE Healthcare) equilibrated in TBS.

Gel electrophoresis analysis

Purified proteins in 4× sample buffer (Invitrogen) were electrophoresed on a 4–12% Bis–Tris gel (Novex, Invitrogen) in MES running buffer. Proteins were then stained with Coomassie brilliant blue.

Surface plasmon resonance

Aβ_{1-16}Im7 binding and kinetics were determined by measuring surface plasmon resonance in a Biacore T100 unit (GE Healthcare). Biotinylated Aβ_{1-16} was coupled to a Series S CM5 research grade chip using *N*-hydroxysuccinimide/*N*-(3-dimethylaminopropyl)-*N*′-ethylcarbodiimide chemistry as described by the manufacturer (GE Healthcare). Unless stated otherwise, all binding experiments were performed at 25°C in triplicate using HBS-EP+ (10 m*M* of 4-(2-hydroxyethyl)-1-piperazineethanesulfonic acid [HEPES], 150 m*M* of NaCl, 3 m*M* of ethylenediaminetetraacetic acid, and 0.05% surfactant P20) as the running buffer.

Complexing

Aβ_{1-16}Im7 was complexed with WO2 Fab at a molar ratio of 1:1. Aβ_{1-16}Im7 (138 μ*M*) was incubated with WO2 Fab (140 μ*M*) in PBS for 2 h at room temperature. The complex was then isolated by size exclusion chromatography using a Superdex 75 column (GE Healthcare) in 10 m*M* of HEPES (pH 7.5), 75 m*M* of NaCl at 0.5 mL/min. Fractions corresponding to the complex were combined and concentrated to at least 6 mg/mL.

Crystallization

Extensive crystallization screening was done at the CSIRO Collaborative Crystallization Centre using an automated nanodrop crystallization facility (http://www.csiro.au/c3). All proteins were set up as 0.4 μL sitting drops at 20°C. Initially, Aβ_{1-16}Im7, concentrated to ~45 mg/mL in 20 m*M* of Tris-HCl (pH 7.5) buffer, was tested in several sets of crystallization trials (672 conditions) using the C3 screen (http://www.csiro.au/c3). For crystallization of Aβ_{1-16}Im7 in complex with WO2 Fab, proteins were initially set up in PEG/Ion (Hampton Research), PACT Premier (Molecular Dimensions), and JCSG plus (Molecular Dimensions) screens with crystal growth favoring PEG 3350. A crystal grown in PEG 3350 (25% w/v), 0.2*M* of $MgCl_2$, 0.1*M* of Bis–Tris (pH 5.5) was used to seed the growth of fast-growing crystals suitable for X-ray diffraction studies using the ionic solution additive screen (Hampton Research). Crystals grew in a variety of conditions with the best diffracting crystal grown in a well solution of 0.2*M* of sodium malonate, 20% (w/v) PEG 3350, 0.1*M* of Bis-Tris propane (pH 8.5), 0.2*M* of 1-methylimidazolium formate.

Structure determination

Diffraction data for a plate-like single crystal (in well solution plus 10% v/v glycerol/10% v/v ethylene glycol as cryoprotectant) were collected at T = 100 K at the Australian synchrotron MX1 beamline[28] with the wavelength of 0.94721 Å. The ADSC Q210 detector was set at a distance of 249 mm, 1° oscillations were taken, and a total of 360 frames were obtained, with each frame given a 1-s total exposure time. The data were processed with HKL2000.[29] Although the data extended up to 2.3 Å of resolution, the completeness of the data fell off owing to diffraction anisotropy and 2.6 Å was considered to be the optimal cutoff point (Table I). The merging statistics were similar for the higher *P2* and lower *P1* space group symmetry. The molecular weight of the complex was 63.1 kDa and the Matthews coefficient, V_m, was 2.25 Å/Da for one or two complexes in the asymmetric unit for possible *P2* or *P1* space group symmetry, respectively. That was equivalent to a solvent content of 45.3%. The search model was built using the Fab fragment of the murine WO2 crystal structure[14] (PDB 3BKJ) with the previously published correct sequence[30] and the Im7 structure[31] (PDB 1AYI). The initial molecular replacement search was conducted in *P2* space group symmetry using PHASER.[32] One complex in the asymmetric unit was identified, then the Aβ_{1-16} fragment was built into the observed residual electron density, and the whole structure was refined using REFMAC[33] to unacceptable high R/R_{free} factors of 0.28/0.33. Concurrently, the Britton plot, *H*-test, and ML estimate performed by XTRIAGE program from the PHENIX[34] crystallography software suite (Supporting Information Fig. S1) suggested three pseudo-merohedral twin operations ($-h,k,-l$; $h,-k,-l$; $-h,-k,l$) with the average twin-fraction estimates of 0.415, 0.079, and 0.087 which were further refined (Table I). The next search was conducted in *P1* space group and two independent complexes were identified in the asymmetric unit by PHASER[32] molecular replacement. Iterative refinement and further model building were conducted using REFMAC[33] and

Table I
Diffraction Data and Refinement Statistics

	$A\beta_{1-16}$Im7–WO2 Fab
Beamline	AS MX1
Wavelength (Å)	0.94721
Space group	*P*1
Twin operators and fractions (α)[a]	(h, k, l), 0.49
	($-h, k, -l$), 0.39
	($-h, -k, l$), 0.12
Unit cell ($a,b,c,\alpha,\beta,\gamma$) (Å, °)	36.6, 82.8, 89.2, 90.1, 92.5, 90.0
Resolution range (Å)	44.56–2.60 (2.64–2.60)[b]
Used unique reflections	28,836
Test reflections[c]	1374
Redundancy	3.3 (2.4)
R_{merged}[d]	0.17 (0.40)
χ^2_{merged}[e]	1.50 (1.16)
$<I/\sigma(I)>$	9.2 (2.0)
Data completeness (%)	89.1 (59.2)
R_{work}[f] (%)	22.6
R_{free}[f] (%)	26.9
RMSD bonds (Å), angles (°)	0.011, 1.587
No. of atoms	8769
$<B>$ (rms)[g] (Å^2)	
Chain A: Im7 + $A\beta_{1-16}$, Im7	61.6(3), 62.2(3)
Chain B: Im7 + $A\beta_{1-16}$, Im7	61.1(3), 62.0(3)
Chain A: $A\beta_{1-9}$, $A\beta_{10-16}$	56.1(3), 61.1(3)
Chain B: $A\beta_{1-9}$, $A\beta_{10-16}$	54.1(3), 60.1(3)
Chain F: $WO2_H$	54.6(3)
Chain H: $WO2_H$	54.7(4)
Chain K: $WO2_L$	54.6(3)
Chain L: $WO2_L$	53.7(4)
Chain W: waters	28.8(2)
Overall	54.9(3)
V_m and corresponding % solvent	2.25, 45.3

[a]Refined in REFMAC.
[b]Values in parenthesis, except for $<B>$, are for the highest shell.
[c]4.7% of the data.
[d]$R_{merge} = \Sigma_{hkl}\Sigma_j |I_j - <I_j>|/\Sigma_{hkl}\Sigma_j |I_j|$,
[e]$\chi^2_{merge} = \Sigma_{hkl}\Sigma_j(I_j - <I_j>)^2/\Sigma_{hkl}\Sigma_j(\sigma_j^2 + <\sigma_j>^2)$, where *hkl* specifies unique indices, *j* indicates equivalent observations of *hkl*, I_j and σ_j^2 are the observed intensities and their errors, and $<I_j>$ and $<\sigma_j>$ are the mean values.
[f]$R = \Sigma_{hkl}||F_o| - F_c|/\Sigma_{hkl}|F_o|$, where F_o and $|F_c|$ are the observed and calculated structure factor amplitudes, respectively.
[g]$<B>$ average *B*-factors include the TLS contribution, except for waters.

XTALVIEW/MIFit,[35,36] and yielded a model for residues 1–102 for $A\beta_{1-16}$Im7 A and B chains, and 1–225 and 1–218 for the WO2 heavy (F and H) and light (K and L) chains, respectively. Additionally, 266 water molecules were identified by difference Fourier methods and refined. The experimental data within $I/\sigma(I) \geq 2$ range with the resolution of 2.6 Å were included in the refinement. Following the convergence in standard REFMAC refinement, further improvement of *R*-factors (>2%) was achieved by refining all chains as separate rigid anisotropic domains with the TLS procedure (transition–libration–screw motion tensors refinement).[37] The final refinement of this model converged to R/R_{free} of about 0.226/0.269 (Table I). Progress of the refinement was monitored using the R_{free} statistics based on a test set encompassing ~5% of the observed diffraction amplitudes.[38] To reduce possible correlations introduced by the twinning, the test reflections were selected in thin-resolution shells. In total, 96.0% of residues were in favored and allowed regions and 4.0% in outlier regions of the Ramachandran plot. The relatively high percentage of residues in the outlier regions reflects the crystal twinning. Supporting Information Figure S2 shows composite omit electron density of $A\beta_{1-16}$ fragments in Chains A and B calculated using COMIT.[39] Further experimental and data processing details are summarized in Table I.

RESULTS

Cloning and expression of $A\beta_{1-16}$Im7

We designed an expression construct, $A\beta_{1-16}$Im7, where the metal-binding residues Asp1–Lys16 of the Aβ peptide were fused to the N-terminus of the Im7 display scaffold. The resulting mature protein lacks both the *Pel*B leader (cleavable N-terminal periplasmic targeting signal removed by secretory pathway processing) and the initiating methionine (mutated to serine). The absence of such extraneous sequences in the vicinity of the Aβ peptide was an important consideration toward our aim of mapping, through a crystallographic approach, the precise contributions of individual Aβ residues to metal binding. The $A\beta_{1-16}$Im7 genetic construct was produced by overlap polymerase chain reaction (for details, see **MATERIALS AND METHODS** section) and cloned into the *E. coli* periplasmic expression vector pGC,[21] incorporating dual C-terminal FLAG affinity purification tags [Fig. 1(a)]. Recombinant protein was purified by FLAG affinity chromatography followed by gel filtration with the majority of protein in the soluble monomeric fraction. Protein was validated by SDS-PAGE [Fig. 1(b)] and by N-terminal amino acid sequencing of the first 20 residues (data not shown). MS modalities were used to confirm the $A\beta_{1-16}$Im7 protein sequence and precise molecular mass of 14,133 Da [Fig. 1(c)].

$A\beta_{1-16}$Im7 complexed with an Aβ-specific antibody

$A\beta_{1-16}$Im7 alone was tested in an extensive range of crystallization trials. Regrettably, no crystal hits were observed, suggesting that the extreme flexibility of the N-terminus was interfering with the formation of crystal contacts. Thus, we next investigated whether $A\beta_{1-16}$Im7 could be partially supported and immobilized by addition of an N-terminal Aβ-specific antibody targeting $A\beta_{3-7}$. We had previously demonstrated that the Fab fragment of the murine antibody WO2 and its humanized equivalents bound Aβ peptide with high affinity.[30] By immobilizing $A\beta_{1-16}$Im7 to a DNase-coated biosensor chip through the underlying Im7 scaffold, we orientated the Aβ epitope away from the surface and measured binding of the WO2 Fab as analyte (Fig. 2). Kinetic and

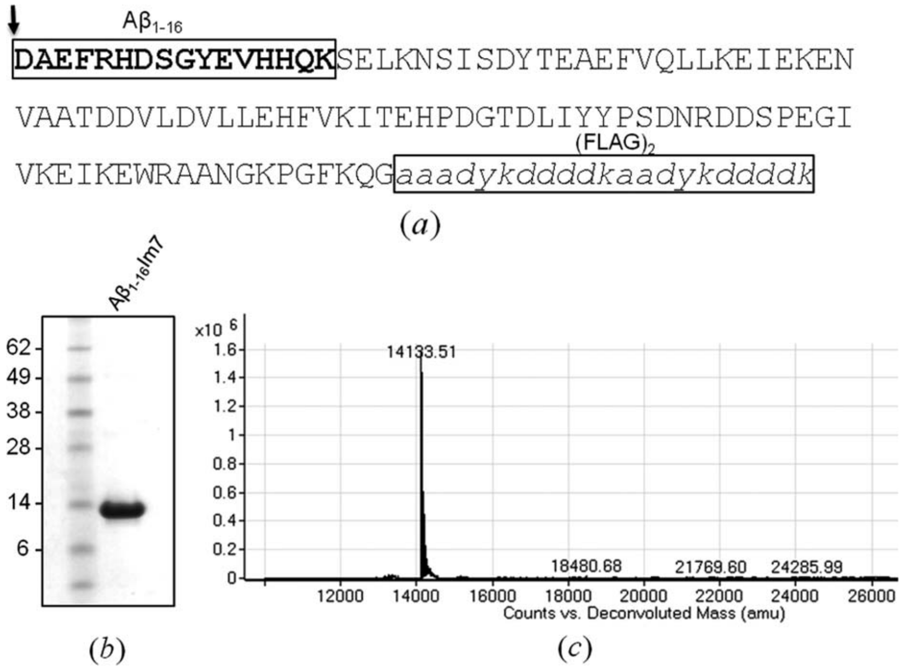

Figure 1

Cloning and expression of $A\beta_{1-16}$Im7. (**a**) $A\beta_{1-16}$Im7 is a single-polypeptide chain of ~14,133 Da including N-terminal Aβ residues 1–16 (boxed and bolded) and dual C-terminal FLAG affinity tags (boxed). The arrow indicates the cleavage site for the *Pel*B signal protease. (**b**) SDS-PAGE illustrating purified $A\beta_{1-16}$Im7. Approximate molecular weights (in kDa) are shown in the left. (*c*) TOF-MS profile of purified $A\beta_{1-16}$Im7 protein.

affinity parameters ($k_a = 1.8 \times 10^5\ M^{-1}\ s^{-1}$; $k_d = 1.0 \times 10^{-3}\ s^{-1}$; $K_D = 5.5 \times 10^{-9} \pm 4.2 \times 10^{-10} M$) correlated well with the interaction between native peptide and the antibody Fab fragment,[30] suggesting that the formation of a ternary complex was possible. Thus, $A\beta_{1-16}$Im7 and WO2 Fab were incubated in solution and size exclusion chromatography was used to measure and confirm complex formation (Fig. 3). The fraction eluting at 9.9 mL was collected, demonstrated to contain both proteins, and entered into crystallization trials.

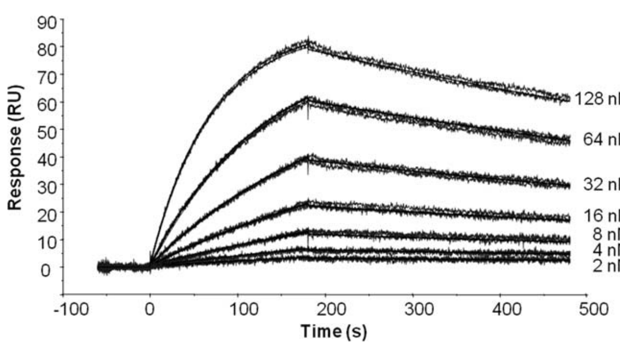

Figure 2

Triplicate data sets for WO2 Fab fragment (128–2 nM) binding to immobilized $A\beta_{1-16}$Im7.

Crystal structure of $A\beta_{1-16}$Im7 complexed with an Aβ-specific antibody

Crystals of various diffraction qualities for $A\beta_{1-16}$Im7–WO2 Fab grew in a variety of conditions (Fig. 3, inset).

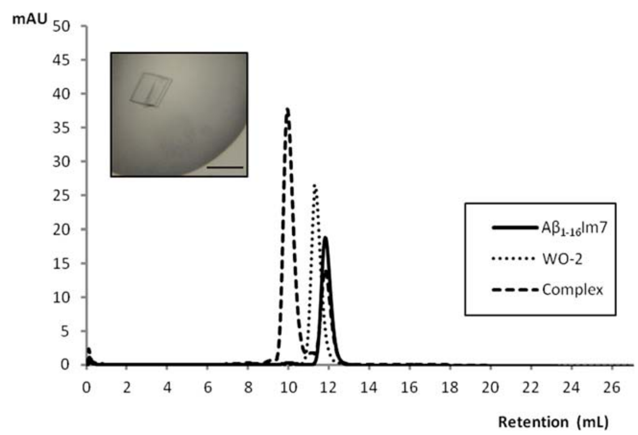

Figure 3

Analysis on Superdex 200 HR 10/30 column of affinity- and gel filtration-purified $A\beta_{1-16}$Im7 protein (solid line) added to WO2 Fab (dotted line). The resultant complex (dashed line) was collected and concentrated for crystallization trials. The inset shows a typical crystal (0.09*M* of $MgCl_2$, 0.01*M* of Bis–Tris propane, pH 6.5, 18% polyethylene glycol 3350, 1-methylimidazolium formate) of the purified complex (scale bar, 200 μm). [Color figure can be viewed in the online issue, which is available at wileyonlinelibrary.com.]

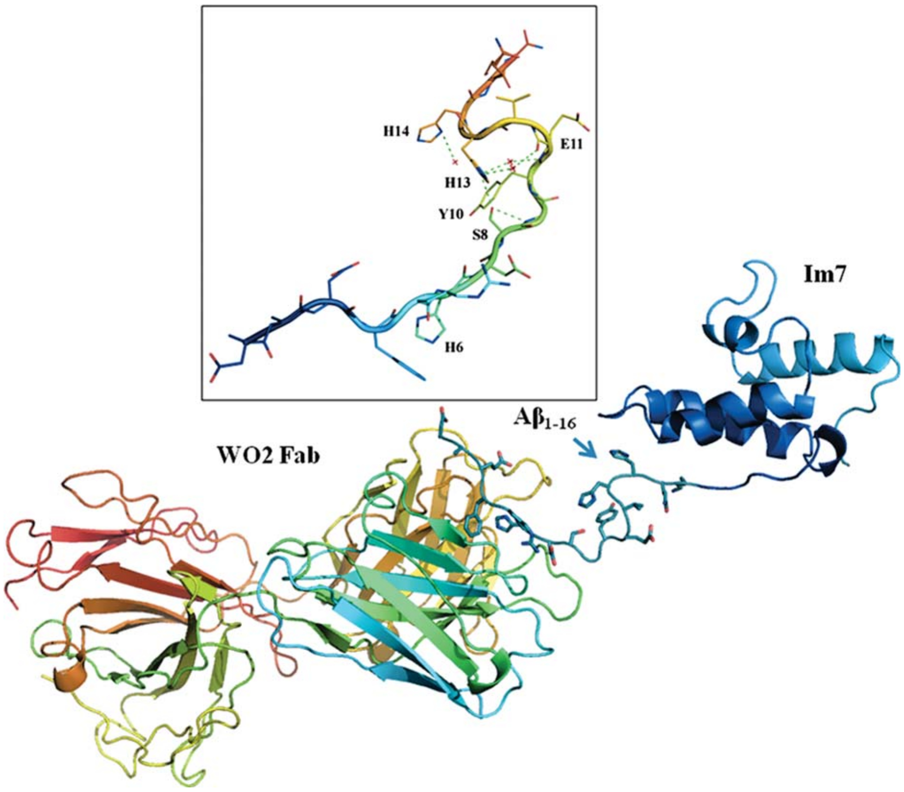

Figure 4

Structure of the $A\beta_{1-16}$Im7–WO2 Fab crystal complex (**a**) and $A\beta_{1-16}$ fragment from Chain A of this structure (contacts $\leq$ 3A involving His13 and His14 are shown with dashed lines) (**b**).

The crystal structure of $A\beta_{1-16}$ constrained by the N-terminal region of Im7 and the WO2 Fab fragment was solved to a resolution of 2.6 Å. In our current model of $A\beta_{1-16}$Im7–WO2 Fab, two complexes occupy the asymmetric unit. The two complexes showed small difference between the two copies with a root-mean-square deviation (r.m.s.d.) of 1.03Å for the Cα atoms from the $A\beta_{1-16}$Im7 molecule (Chains A and B), of 1.12 Å for 225 Cα atoms from the Fab heavy Chains F and H, and of 0.96Å for the 218 Cα atoms from the Fab light Chains K and L. The two independent complexes were rotated with respect to each other by 179 (1)° about *b*-axis coupled with a translation of approximately (0.005, −0.495, and 1.005). Although the main fraction twinning operator was parallel to the rotation along *b*-axis, the rotation axis deviated slightly from the exact crystallographic twofold axis. The murine WO2 Fab structure was closely superimposed with the published murine WO2 structure[14] (PDB 3BKJ) with r.m.s.d on Cα atoms of 0.78 and 1.24 Å for variable and constant domains of heavy chain, respectively, and of 0.61 and 1.21 Å for variable and constant domains of light chain, respectively. The Im7 scaffold (residues, 17–102) also superimposed closely (r.m.s.d., 1.18 Å) with the known structure[31] (PDB 1AYI). In contrast to the previous structures,[14] we were now able to observe all 1–16 residues with reasonably defined electron density (Supporting Information Fig. S2). The structure of the slightly better defined $A\beta_{1-16}$Im7–WO2 Fab crystal complex (Chains A, H, and L) is shown in Figure 4. The WO2 Fab bound the immunodominant B-cell epitope between residues 2 and 8 of Aβ. Residues 2–8 of the Aβ fragment were occluded and "straightened" by the antibody and their superposition from our Chain A and published structures[14] yielded r.m.s.d. of 0.79 Å. The mean temperature factors for the $A\beta_{1-9}$ fragment were close to the mean temperature factors for the Fab (Table I) as would be expected for the interaction with the Fab epitope segment from Ala2 to Ser8. The $A\beta_{10-16}$ fragments had slightly larger temperature factors but still in the range of temperature factors for the rest of the Aβ-Im7 Chains (Table I), indicating that the segments of interest, A_{10-16}, were moderately rigid and formed ordered structures. Table II summarizes backbone dihedral angles for the $A\beta_{10-16}$ segments of Chains A and B, and various approaches used for secondary structure assignment, which relied on different descriptors. In general, the structure descriptions in the most commonly used DSSP[40] or STRIDE[41] algorithms were limited to three classes: α-helix, β-strand, and a state corresponding to other regions in the backbone, the

Table II
Backbone Dihedral Angles for the Aβ_{10-16} Segment from Chain A

No.	AA	φ (°)	ψ (°)	PROSS	STRIDE	DSSP
10	TYR	−73.7	−38.7	Coil	Turn	Bent
11	GLU	153.6	−114.2	Coil	Turn	Bent
12	VAL	−86.1	163.8	PPII	Turn	Bent
13	HIS	−93.0	123.3	PPII	Turn	Bent
14	HIS	51.3	112.0	Coil	Turn	Bent
15	GLN	−167.7	153.8	Coil	Turn	Coil
16	LYS	−129.7	127.78	Coil	Coil	Coil

coil, and under-represented PPII-helix, whereas PROSS[42] seemed more sensitive to PPII-helix-type conformations.[43] According to a recent approach[43] for secondary structure assignment, at least two consecutive residues with dihedral angles within the range ($\varphi = -75.3 \pm 29°$, $\psi = 141.1 \pm 29°$) were required to form a PPII-helix. The dihedral angles for Val12 and His13 of Chain A in Table II were well within that range, suggesting that Aβ_{10-16} had a propensity to form the PPII-helix. Assignment made by PROSS was based solely on backbone angles, mainly involving the φ and ψ dihedral angles. In addition to the hydrogen bond criteria used by the more common DSSP algorithm, the STRIDE assignment criteria also included dihedral angle potentials and defined the Aβ_{10-16} peptide structure mainly as a turn (Table II). A further important feature of the Aβ_{10-16} fragment was that residues His13 and His14 appeared to reside on the tip of the turn/PPII-helix structure formed by residues 10–16. This turn could be stabilized by interactions of His13 with Ser8 directly and with Glu11 via waters in Chain A (Fig. 4, inset). The first-principle molecular dynamics simulations[44] suggested that hydrogen bonding between Val12 and Gln15 was also possible, though weak. The His14 $N_{\delta 1}$ atom was involved in the H-bond of 2.9 Å with a water molecule which could be expected at the pH used for crystal growth. The unprotonated $N_{\delta 1}$ in the anionic τ tautomeric state of histidine at pH 8.5 could serve as an H-bond acceptor.[45] It was interesting to note that a simple change of side-chain rotamers for residues His13 and His14 can create an ideal configuration of imidazole rings for metal coordination. However, none of the other side chains of residues in close proximity to these two histidines, including Tyr10 (Fig. 4), could be adjusted through rotamers to become metal-binding ligands. This suggests that the involvement of residues other than His13 and His14 in metal binding may depend on conditions (e.g., pH, buffers, and temperature) modulating the unstructured N-terminal residues 1–10.

In a preliminary attempt to further clarify metal binding in our system, cocrystallization and soaking experiments were performed for Aβ_{1-16}Im7–WO2 Fab complexes with Zn^{2+} ions. The excitation scans verified the presence of Zn ions in the crystals; however, consistently-low resolution diffraction data (∼4.0 Å) precluded accurate structure analysis.

DISCUSSION

Although the exact mechanism of neurotoxicity in AD has not been clearly defined, Aβ is a widely accepted therapeutic target. The N-terminus of Aβ is particularly attractive owing to its metal-binding properties and accessibility upon aggregation, highlighted by the observation that only anti-Aβ antibodies raised against the N-terminus of Aβ can prevent both Aβ aggregation and dissociate existing Aβ fibrils.[30] Precise structural information for Aβ to facilitate the development of therapeutics is limited, however, in part owing to the difficulty of stabilizing the Aβ monomer for crystallization. Here, we partially resolved this bottleneck by utilizing the Im7 immunity protein as an efficient scaffold for the stabilization of Aβ_{1-16}, in combination with complex formation using the Aβ-specific WO2 Fab. This protein engineering approach allowed us to report the 2.6-Å resolution crystal structure of Aβ residues 1–16 neatly tethered between the N-terminal antibody and the Im7 protein scaffold.

Previous solution studies of the N-terminus of Aβ suggested that the first 9–10 residues were poorly structured, whereas residues beyond 10 formed defined structures.[3–11] Consistent with those studies, we showed using X-ray crystallography that residues 10–16 of Aβ formed a mixture of turn/PPII-helix-type conformations with adjacent residues His13 and His14 residing on the tip of the turn. PPII is thought to be a predominant backbone conformation in peptides as it is extended, flexible, lacks intrachain hydrogen bonds, and is fully hydrated in aqueous solution.[46] As it is close in conformation to a β-strand, it would be expected to readily undergo conformational change and aggregation in appropriate conditions. As such, PPII-helices have the appropriate characteristics to be implicated as critical conformational elements in many conformational diseases.[12]

Here, adjacent residues His13 and His 14 were of particular interest as they are thought to form a significant component of the Aβ metal-binding epitope. Although the exact coordination of Cu^{2+}, Zn^{2+}, and Fe^{2+} to Aβ is still unknown, studies suggested that they coordinate with the three histidines in the Aβ N-terminus (His6, His13, and His14). Other ligands were most likely either the amino group of the N-terminus or the carboxylate from Asp1, Glu3, or Glu11 or the carbonyl from Ala2,[47–51] whereas occasionally, a water molecule was also proposed.[49,52,53] This inability to precisely define the exact metal coordination geometry in Aβ suggested that metal coordination might be pleomorphic[54] though with some preference to His13 and His14 residues. The His13-Cu^{1+}–His14 linear coordination is favored by interactions present in the complete solvated and *in vacuo* models of $A\beta_{1-16}Cu^{1+}$ investigated by the first-principle molecular dynamic simulations in the Car–Parrinello scheme.[44] This simulation revealed two separated 1–10 and 11–16 peptide regions. The presence of a flexible junction between these regions, together with the relative rigid region 11–16, made the cooperation between His13 and His14 more favorable than the cooperation between His 6 and His13 or His 14 residues belonging to the two different regions. The regions 11–16 appeared as an almost independent unit trapping metal ions.[44] The three-pulse electron spin-echo envelope modulation spectra of the $A\beta_{1-16}Cu^{2+}$ complexes indicated that the simultaneous coordination by the two adjacent His13–His14 residues is likely to be present in a non-β-sheet structure of small oligomers.[55]

In addition to enhancing the aggregation behavior of Aβ, Aβ–Cu and Aβ–Fe complexes are involved in extensive redox chemical reactions, facilitated by reducing agents, for example ascorbates, which catalytically produce reactive oxygen species from molecular oxygen.[56,57] Accordingly, MS demonstrated that Cu^{2+}/Cu^{1+}-triggered redox chemistry was able to oxygenate Aβ at a number of different residues: primarily His13 and His14 and to a lesser extent His6 and Met35.[58–60] Considering that the Cu^{1+} was predominantly coordinated by the imidazole groups of two histidine residues His13 and His14 in a linear fashion,[44,55,61–63] these results emphasized that His13 and His14 are the two most firmly established ligands in the coordination sphere of the Cu^{1+} and Cu^{2+} ions bound to Aβ. In particular, the importance of His14 is further emphasized by toxicity studies,[64] which indicate that this residue additionally facilitates membrane binding and neurotoxicity of Aβ.

We hypothesise that the relatively rigid turn/PPII-helix conformation formed by residues 10–16 and trapped in our crystal structure is important for the initial metal binding and stabilization of the monomeric and potentially oligomeric states, leading to small oligomer formation toward a pathogenic species. Combining our two crystallographic structures of N-terminal Aβ peptide residues Asp1–Lys16 (presented here) and of the C-terminal Aβ amyloidogenic residues Val18–Ile41 in the most stable homodimer form[17] resulted in a model (Fig. 5) whereby the metal-binding site and in particular the His13 and His14 residues were ideally oriented to mediate reactive oxygen species toxicity and modulate membrane binding. In a membranous environment, as shown in Figure 5, an $A\beta_{1-42}$ dimer exposed the N-terminal metal-binding sites while burying hydrophobic residues (C-terminal β-sheets) in a hydrophobic milieu. Such an arrangement would place the turn/PPII-helix formed by residues 10–16 in close proximity to the charged loops formed by the C-terminal components of the $A\beta_{1-42}$ dimer and in a position to potentially interact with

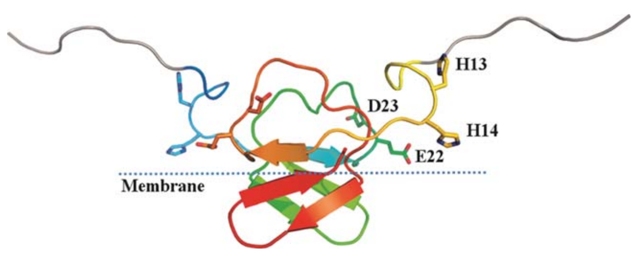

Figure 5

Model of a nonfibrillar $A\beta_{1-42}$ dimer by combining crystallographic structures of $A\beta_{1-16}$ and $A\beta_{18-41}$[17] fragments. Residues Leu17 and Ala42 as well as $A\beta_{1-16}$ fragment were added to preserve and extend β-sheets of the $A\beta_{18-41}$ structure. Residues 1–8 involved in interaction with WO2 Fab are shown in gray. The hydrophobic dimer–dimer interface of the $A\beta_{1-42}$ tetramer is intercalated into the membrane (dashed line) surface through nonelectrostatic interactions, whereas hydrophilic aspects with metal binding sites are on the membrane surface.

Glu22 or even Asp23 across the dimer interface (Fig. 5). Thus, as an alternative to the potential Asp1/Glu3/Glu11 metal ligands,[47–4951,54] residues Glu22 and/or Asp23 could be involved in metal coordination across the dimer interface stabilizing the dimeric oligomer. Within this context, it is not insignificant that residues Glu22 and Asp23 are implicated in a major cluster of pathogenic familiar AD mutations,[65] for example Glu22Gly (Arctic), Glu22Gln (Dutch), Glu22Lys (Italian), and Asp23Asn (Iowa). Based on these studies, it is, therefore, not surprising that modulating the N-terminus of Aβ inhibits its neurotoxic activity. Antibodies raised against the N-terminus of Aβ were shown to effectively dissociate Aβ aggregates *in vitro* and in clinical trials providing evidence that this region of Aβ was accessible within aggregates.[15] Methylation of the imidazole side chains on the three histidines of Aβ inhibited neurotoxicity of Aβ *in vitro*,[66,67] and binding of platinum compounds to the metal binding site of Aβ inhibited neurotoxicity and rescued Aβ-induced synaptotoxicity in mouse hippocampal slices.[68] Furthermore, Tyr10 could be targeted to prevent the formation of the putative di-Tyr-linked Aβ dimers, which were shown to be neurotoxic.[69] These studies highlighted the potential of residues 10–16 of Aβ as an AD therapeutic target.

CONCLUSIONS

In summary, the novel structure presented here illustrates a potential target for the development of future AD therapeutics aimed at stabilizing the N-terminal monomer structure, in particular residues His13 and His14, and preventing Aβ metal-binding-induced neurotoxicity. From a practical perspective, analysis of the crystal packing suggests that the crystallographic forms obtained here may accommodate small molecules, and therefore have utility in drug discovery strategies involving compound screening and fragment soaking methodologies. Such approaches represent, once the not insignificant challenges of obtaining high-quality crystallographic data sets for various metals complexes are overcome, viable pathways to the development of small-molecule drugs toward eventual amelioration of AD.

ACKNOWLEDGMENTS

The authors acknowledge the use of the CSIRO Collaborative Crystallization Centre (C3), and the MX1 beamline at the Australian Synchrotron, Victoria, Australia. The authors thank Dr. Janet Newman (C3) for her advice on crystallization and Mr. Nick Bartone for mass spectrometry data. Coordinates and structural parameters for Aβ_{1-16}Im7–WO2 Fab complex have been deposited with the Protein Data Bank under accession code: 4F37. The authors have no conflicts of interest to declare.

REFERENCES

1. Shankar GM, Li S, Mehta TH, Garcia-Munoz A, Shepardson NE, Smith I, Brett FM, Farrell MA, Rowan MJ, Lemere CA, Regan CM, Walsh DM, Sabatini BL, Selkoe DJ. Amyloid-beta protein dimers isolated directly from Alzheimer's brains impair synaptic plasticity and memory. Nat Med 2008;14:837–842.
2. Walsh DM, Klyubin I, Fadeeva JV, Cullen WK, Anwyl R, Wolfe MS, Rowan MJ, Selkoe DJ. Naturally secreted oligomers of amyloid beta protein potently inhibit hippocampal long-term potentiation in vivo. Nature 2002;416:535–539.
3. Petkova AT, Ishii Y, Balbach JJ, Antzutkin ON, Leapman RD, Delaglio F, Tycko R. A structural model for Alzheimer's b-amyloid fibrils based on experimental constraints from solid state NMR. Proc Natl Acad Sci USA 2002;99:16742–16747.
4. Crescenzi O, Tomaselli S, Guerrini R, Salvadori S, D'Ursi AM, Temussi PA, Picone D. Solution structure of the Alzheimer amyloid beta-peptide (1-42) in an apolar microenvironment. Similarity with a virus fusion domain. Eur J Biochem 2002;269:5642–5648.
5. Coles M, Bicknell W, Watson AA, Fairlie DP, Craik DJ. Solution structure of amyloid beta-peptide(1-40) in a water-micelle environment. Is the membrane-spanning domain where we think it is? Biochemistry 1998;37:11064–11077.
6. Shao H, Jao S, Ma K, Zagorski MG. Solution structures of micelle-bound amyloid beta-(1-40) and beta-(1-42) peptides of Alzheimer's disease. J Mol Biol 1999;285:755–773.
7. Sticht H, Bayer P, Willbold D, Dames S, Hilbich C, Beyreuther K, Frank RW, Rosch P. Structure of amyloid A4-(1-40)-peptide of Alzheimer's disease. Eur J Biochem 1995;233:293–298.
8. Barrow CJ, Zagorski MG. Solution structures of beta peptide and its constituent fragments: relation to amyloid deposition. Science 1991;253:179–182.
9. Jarvet J, Damberg P, Danielsson J, Johansson I, Eriksson LEG, Gräslund A. A left-handed 31 helical conformation in the Alzheimer Aβ(12–28) peptide. FEBS Lett 2003;555:371–374.
10. Danielsson J, Andersson A, Jarvet J, Gräslund A. 15N relaxation study of the amyloid β-peptide: structural propensities and persistence length. Magn Reson Chem 2006;44:S114–S121.
11. Eker F, Griebenow K, Schweitzer-Stenner R. Abeta(1-28) fragment of the amyloid peptide predominantly adopts a polyproline II conformation in an acidic solution. Biochemistry 2004;43:6893–6898.
12. Blanch EW, Morozova-Roche LA, Cochran DAE, Doig AJ, Hecht L, Barron LD. Is polyproline II helix the killer conformation? a raman optical activity study of the amyloidogenic prefibrillar intermediate of human lysozyme. J Mol Biol 2000;301:553–563.
13. Gardberg AS, Dice LT, Ou S, Rich RL, Helmbrecht E, Ko J, Wetzel R, Myszka DG, Patterson PH, Dealwis C. Molecular basis for passive immunotherapy of Alzheimer's disease. Proc Natl Acad Sci USA 2007;104:15659–15664.
14. Miles LA, Wun KS, Crespi GA, Fodero-Tavoletti MT, Galatis D, Bagley CJ, Beyreuther K, Masters CL, Cappai R, McKinstry WJ, Barnham KJ, Parker MW. Amyloid-β-anti-amyloid-β complex structure reveals an extended conformation in the immunodominant B-cell epitope. J Mol Biol 2008;377:181–192.
15. Miles LA, Crespi GAN, Doughty L, Parker MW. Bapineuzumab captures the N-terminus of the Alzheimer's disease amyloid-beta peptide in a helical conformation. Sci Rep 2013;3:1302.
16. Takano K, Endo S, Mukaiyama A, Chon H, Matsumura H, Koga Y, Kanaya S. Structure of amyloid-β fragments in aqueous environments. FEBS J 2006;273:150–158.
17. Streltsov VA, Varghese JN, Masters CL, Nuttall SD. Crystal structure of the amyloid-beta p3 fragment provides a model for oligomer formation in Alzheimer's disease. J Neurosci 2011;31:1419–1426.
18. Chak KF, Safo MK, Ku WY, Hsieh SY, Yuan HS. The crystal structure of the immunity protein of colicin E7 suggests a possible colicin-interacting surface. Proc Natl Acad Sci USA 1996;93:6437–6442.
19. Juraja SM, Mulhern TD, Hudson PJ, Hattarki MK, Carmichael JA, Nuttall SD. Engineering of the *Escherichia coli* Im7 immunity protein as a loop display scaffold. Protein Eng Des Sel 2006;19:231–244.
20. Hosse RJ, Tay L, Hattarki MK, Pontes-Braz L, Pearce LA, Nuttall SD, Dolezal O. Kinetic screening of antibody-Im7 conjugates by capture on a colicin E7 DNase domain using optical biosensors. Anal Biochem 2009;385:346–357.
21. Coia G, Ayres A, Lilley GG, Hudson PJ, Irving RA. Use of mutator cells as a means for increasing production levels of a recombinant antibody directed against Hepatitis B. Gene 1997;201:203–209.
22. Nuttall SD, Krishnan UV, Doughty L, Nathanielsz A, Ally N, Pike RN, Hudson PJ, Kortt AA, Irving RA. A naturally occurring NAR variable domain binds the Kgp protease from *Porphyromonas gingivalis.* FEBS Lett 2002;516:80–86.
23. Minsky A, Summers RG, Knowles JR. Secretion of beta-lactamase into the periplasm of *Escherichia coli*: evidence for a distinct release step associated with a conformational change. Proc Natl Acad Sci USA 1986;83:4180–4184.
24. Nuttall SD, Humberstone KS, Krishnan UV, Carmichael JA, Doughty L, Hattarki M, Coley AM, Casey JL, Anders RF, Foley M, Irving RA, Hudson PJ. Selection and affinity maturation of IgNAR variable domains targeting *Plasmodium falciparum* AMA1. Proteins 2004;55:187–197.
25. Robert R, Dolezal O, Waddington L, Hattarki MK, Cappai R, Masters CL, Hudson PJ, Wark KL. Engineered antibody intervention strategies for Alzheimer's disease and related dementias by targeting amyloid and toxic oligomers. Protein Eng Des Sel 2009;22:199–208.
26. Ida N, Hartmann T, Pantel J, Schroder J, Zerfass R, Forstl H, Sandbrink R, Masters CL, Beyreuther K. Analysis of heterogeneous A4 peptides in human cerebrospinal fluid and blood by a newly developed sensitive Western blot assay. J Biol Chem 1996;271:22908–22914.
27. Gruen LC, Kortt AA, Nice E. Determination of relative binding affinity of influenza virus N9 sialidases with the Fab fragment of monoclonal antibody NC41 using biosensor technology. Eur J Biochem 1993;217:319–325.
28. McPhillips TM, McPhillips SE, Chiu HJ, Cohen AE, Deacon AM, Ellis PJ, Garman E, Gonzalez A, Sauter NK, Phizackerley RP, Soltis SM, Kuhn P. Blu-Ice and the Distributed Control System: software for data acquisition and instrument control at macromolecular crystallography beamlines. J Synchrotron Radiat 2002;9:401–406.

29. Otwinowski Z, Minor W. Processing of X-ray diffraction data collected in oscillation mode. Methods Enzymol 1997;276:307–326.
30. Robert R, Streltsov VA, Newman J, Pearce LA, Wark KL, Dolezal O. Germline humanization of a murine Abeta antibody and crystal structure of the humanized recombinant Fab fragment. Protein Sci 2009;19:299–308.
31. Dennis CA, Videler H, Pauptit RA, Wallis R, James R, Moore GR, Kleanthous C. A structural comparison of the colicin immunity proteins Im7 and Im9 gives new insights into the molecular determinants of immunity-protein specificity. Biochem J 1998;333:183–191.
32. McCoy AJ, Grosse-Kunstleve RW, Adams PD, Winn MD, Storoni LC, Read RJ. Phaser crystallographic software. J Appl Crystallogr 2007;40:658–674.
33. Murshudov GN, Vagin AA, Dodson EJ. Refinement of macromolecular structures by the maximum-likelihood method. Acta Crystallogr 1997;D53:240–255.
34. Adams PD, Afonine PV, Bunkoczi G, Chen VB, Davis IW, Echols N, Headd JJ, Hung LW, Kapral GJ, Grosse-Kunstleve RW, McCoy AJ, Moriarty NW, Oeffner R, Read RJ, Richardson DC, Richardson JS, Terwilliger TC, Zwart PH. PHENIX: a comprehensive Python-based system for macromolecular structure solution. Acta Crystallogr D Biol Crystallogr 2010;66:213–221.
35. McRee DE. XtalView/Xfit-A versatile program for manipulating atomic coordinates and electron density. J Struct Biol 1999;125:156–165.
36. McRee DE, Badger J. MIFit Manual Version 30 for Windows and LINUX© Rigaku 2003-6.
37. Winn MD, Isupov MN, Murshudov GN. Use of TLS parameters to model anisotropic displacements in macromolecular refinement. Acta Crystallogr D Biol Crystallogr 2001;57:122–133.
38. Brünger AT. The Free R value: a novel statistical quantity for assessing the accuracy of crystal structures. Nature 1992;355:472–474.
39. Winn MD, Ballard CC, Cowtan KD, Dodson EJ, Emsley P, Evans PR, Keegan RM, Krissinel EB, Leslie AGW, McCoy A, McNicholas SJ, Murshudov GN, Pannu NS, Potterton EA, Powell HR, Read RJ, Vagin A, Wilson KS. Overview of the CCP4 suite and current developments. Acta Crystallogr D 2011;67:235–242.
40. Kabsch W, Sander C. Dictionary of protein secondary structure: pattern recognition of hydrogen-bonded and geometrical features. Biopolymers 1983;22:2577–2637.
41. Frishman D, Argos P. Knowledge-based protein secondary structure assignment. Proteins 1995;23:566–579.
42. Srinivasan R, Rose GD. A physical basis for protein secondary structure. Proc Natl Acad Sci USA 1999;96:14258–14263.
43. Mansiaux Y, Joseph AP, Gelly JC, de Brevern AG. Assignment of PolyProline II conformation and analysis of sequence—structure relationship. PLoS One 2011;6:e18401.
44. Furlan S, Hureau C, Faller P, La Penna G. Modeling the Cu+ binding in the 1-16 region of the amyloid-beta peptide involved in Alzheimer's disease. J Phys Chem B 2010;114:15119–15133.
45. Li S, Hong M. Protonation, tautomerization, and rotameric structure of histidine: a comprehensive study by magic-angle-spinning solid-state NMR. J Am Chem Soc 2011;133:1534–1544.
46. Jha AK, Colubri A, Zaman MH, Koide S, Sosnick TR, Freed KF. Helix, sheet, and polyproline II frequencies and strong nearest neighbor effects in a restricted coil library. Biochemistry 2005;44:9691–9702.
47. Karr JW, Akintoye H, Kaupp LJ, Szalai VA. N-Terminal deletions modify the Cu2+ binding site in amyloid-beta. Biochemistry 2005;44:5478–5487.
48. Stellato F, Menestrina G, Serra MD, Potrich C, Tomazzolli R, Meyer-Klaucke W, Morante S. Metal binding in amyloid beta-peptides shows intra- and inter-peptide coordination modes. Eur Biophys J 2006;35:340–351.
49. Streltsov V, Titmuss S, Epa V, Barnham K, Masters C, Varghese J. The structure of the amyloid-β peptide high-affinity copper II binding site in Alzheimer disease. Biophys J 2008;95:3447–3456.
50. Drew SC, Masters CL, Barnham KJ. Alanine-2 carbonyl is an oxygen ligand in Cu2+ coordination of Alzheimer's disease amyloid-beta peptide—relevance to N-terminally truncated forms. J Am Chem Soc 2009;131:8760–8761.
51. Bousejra-ElGarah F, Bijani C, Coppel Y, Faller P, Hureau C. Iron(II) binding to amyloid-beta, the Alzheimer's peptide. Inorg Chem 2011;50:9024–9030.
52. Yu H, Ren J, Qu X. Different hydration changes accompanying copper and zinc binding to amyloid beta-peptide: water contribution to metal binding. Chembiochem 2008;9:879–882.
53. Tsvetkov PO, Kulikova AA, Golovin AV, Tkachev YV, Archakov AI, Kozin SA, Makarov AA. Minimal Zn(2+) binding site of amyloid-beta. Biophys J 2010;99:L84–L86.
54. Drew SC, Noble CJ, Masters CL, Hanson GR, Barnham KJ. Pleomorphic copper coordination by Alzheimer's disease amyloid-beta peptide. J Am Chem Soc 2009;131:1195–1207.
55. Shin BK, Saxena S. Substantial contribution of the two imidazole rings of the His13-His14 dyad to Cu(II) binding in amyloid-beta(1-16) at physiological pH and its significance. J Phys Chem A 2011;115:9590–9602.
56. Barnham KJ, Masters CL, Bush AI. Neurodegenerative diseases and oxidative stress. Nat Rev Drug Discov 2004;3:205–214.
57. Streltsov VA, Varghese JN. Substrate mediated reduction of copper-amyloid-β complex in Alzheimer's disease. Chem Commun 2008:3169–3171.
58. Atwood CS, Huang X, Khatri A, Scarpa RC, Kim YS, Moir RD, Tanzi RE, Roher AE, Bush AI. Copper catalyzed oxidation of Alzheimer Abeta. Cell Mol Biol (Noisy-le-grand) 2000;46:777–783.
59. Schoneich C. Redox processes of methionine relevant to beta-amyloid oxidation and Alzheimer's disease. Arch Biochem Biophys 2002;397:370–376.
60. Barnham KJ, Ciccotosto GD, Tickler AK, Ali FE, Smith DG, Williamson NA, Lam YH, Carrington D, Tew D, Kocak G, Volitakis I, Separovic F, Barrow CJ, Wade JD, Masters CL, Cherny RA, Curtain CC, Bush AI, Cappai R. Neurotoxic, redox-competent Alzheimer's beta-amyloid is released from lipid membrane by methionine oxidation. J Biol Chem 2003;278:42959–42965.
61. Himes RA, Park GY, Siluvai GS, Blackburn NJ, Karlin KD. Structural studies of copper(I) complexes of amyloid-beta peptide fragments: formation of two-coordinate bis(histidine) complexes. Angew Chem Int Ed Engl 2008;47:9084–9087.
62. Shearer J, Szalai VA. The amyloid-beta peptide of Alzheimer's disease binds Cu(I) in a linear bis-his coordination environment: insight into a possible neuroprotective mechanism for the amyloid-beta peptide. J Am Chem Soc 2008;130:17826–17835.
63. Hureau C, Balland V, Coppel Y, Solari PL, Fonda E, Faller P. Importance of dynamical processes in the coordination chemistry and redox conversion of copper amyloid-beta complexes. J Biol Inorg Chem 2009;14:995–1000.
64. Smith DG, Ciccotosto GD, Tew DJ, Perez K, Curtain CC, Boas JF, Masters CL, Cappai R, Barnham KJ. Histidine 14 modulates membrane binding and neurotoxicity of the Alzheimer's disease amyloid-beta peptide. J Alzheimers Dis 2010;19:1387–1400.
65. Betts V, Leissring MA, Dolios G, Wang R, Selkoe DJ, Walsh DM. Aggregation and catabolism of disease-associated intra-Aβ mutations: reduced proteolysis of AβA21G by neprilysin. Neurobiol Dis 2008;31:442–450.
66. Smith DP, Smith DG, Curtain CC, Boas JF, Pilbrow JR, Ciccotosto GD, Lau TL, Tew DJ, Perez K, Wade JD, Bush AI, Drew SC, Separovic F, Masters CL, Cappai R, Barnham KJ. Copper-mediated amyloid-β toxicity is associated with an intermolecular histidine bridge. J Biol Chem 2006;281:15145–15154.
67. Tickler AK, Smith DG, Ciccotosto GD, Tew DJ, Curtain CC, Carrington D, Masters CL, Bush AI, Cherny RA, Cappai R, Wade JD,

Barnham KJ. Methylation of the imidazole side chains of the Alzheimer disease amyloid-beta peptide results in abolition of superoxide dismutase-like structures and inhibition of neurotoxicity. J Biol Chem 2005;280:13355–13363.

68. Barnham KJ, Kenche VB, Ciccotosto GD, Smith DP, Tew DJ, Liu X, Perez K, Cranston GA, Johanssen TJ, Volitakis I, Bush AI, Masters CL, White AR, Smith JP, Cherny RA, Cappai R. Platinum-based inhibitors of amyloid-beta as therapeutic agents for Alzheimer's disease. Proc Natl Acad Sci USA 2008;105:6813–6818.
69. Atwood CS, Perry G, Zeng H, Kato Y, Jones WD, Ling KQ, Huang X, Moir RD, Wang D, Sayre LM, Smith MA, Chen SG, Bush AI. Copper mediates dityrosine cross-linking of Alzheimer's amyloid-beta. Biochemistry 2004;43:560–568.